JOURNAL OF AIRCRAFT
Vol. 42, No. 3, May–June 2005

Delta Wing Stall and Roll Control Using Segmented Piezoelectric Fluidic Actuators

S. Margalit,* D. Greenblatt,† A. Seifert,‡ and I. Wygnanski§
Tel-Aviv University, 69978 Tel-Aviv, Israel

The separated flow around a balance-mounted, 60-deg sweptback, semispan delta wing with a sharp leading edge was controlled using zero-mass-flux periodic excitation from a segmented leading-edge slot. Excitation was generated by cavity-installed piezoelectric actuators operating at resonance with amplitude modulation (AM) and burst mode (BM) signals being used to achieve reduced frequencies (scaled with the freestream velocity and the root chord) in the range from $\mathcal{O}(1)$ to $\mathcal{O}(10)$. Results of a parametric investigation, studying the effects of AM frequency, BM duty cycle and frequency, excitation amplitude, location of the actuation along the leading edge, and optimal phase difference between the actuators, as well as the Reynolds number, are reported and discussed. Balance data were supplemented by upper surface static pressure measurements and particle image velocimetry (PIV) data. Order unity reduced-frequency modulation of the high-frequency carrier wave increased the normal force generated by the delta wing most effectively. BM with a duty cycle that was as low as 5% was more effective than the amplitude-modulated signal with larger peak excitation velocity and an order of magnitude larger momentum input. PIV data suggest that excitation enhances the momentum transfer across the shear layer, downstream of the original vortex breakdown location, generating a streamwise vortex the size of which is commensurate with the local wing span.

Nomenclature

A_i	=	exit area of ith slot
A_w	=	wing plan view area
B_{te}	=	wing span
b	=	local wing span
b'	=	local maximum normal distance from the leading edge
C_D	=	drag force coefficient, D/qA_w
C_E	=	input power coefficient, $W/qU_\infty A_w$
C_L	=	lift force coefficient, L/qA_w
$C_{L\max}$	=	maximum lift coefficient
C_M	=	pitching moment coefficient, M_P/qA_wc
C_N	=	normal force coefficient, N/qA_w
C_P	=	local pressure coefficient, $(p-p_\infty)/q$
C_R	=	rolling moment coefficient, M_R/qA_wc
C_μ	=	excitation momentum coefficient, $\sum_{i=1}^{K}\rho u_i'^2 A_i \Big/ \frac{1}{2}\rho U_\infty^2 A_w$
c	=	root chord
c'	=	leading-edge length
D	=	drag force
DCy	=	duty cycle, nf_m/f_r
FM	=	figure of merit, $\eta/(C_L/C_D)_{\text{baseline}}$
F^+	=	nondimensional excitation frequency, (fc/U_∞)
f	=	excitation frequency; either f_m or f_r, depends on excitation type
f_m	=	modulating frequency
f_r	=	actuators resonance frequency
K	=	number of active actuator elements
L	=	length of separated region
n	=	number of excitation cycles
p	=	local pressure
Q	=	in-plane velocity, $\sqrt{(w^2+v^2)}$
q	=	freestream dynamic pressure, $\rho U_\infty^2/2$
Re	=	root chord Reynolds number, $U_\infty c/\nu$
T_m	=	input signal modulation period
T_r	=	period of actuators' sine wave
U_p	=	slot exit peak velocity
U_∞	=	freestream velocity
$\langle u\rangle_f$	=	fast Fourier transform amplitude results at $f=f_m$
u'	=	rms of velocity fluctuations
u_s'	=	u' at the slot's exit
V_{rms}	=	rms excitation voltage
v, w	=	velocity components of the flow in the y, z directions
W	=	actuator input power, W
X_R	=	distance from actuator to reattachment area
X_{TE}	=	distance from actuator to trailing edge
x, y, z	=	Cartesian coordinates, (Fig. 1)
x', y'	=	rotated coordinates, (Fig. 1)
α	=	angle of attack
α_s	=	stall α
η	=	aerodynamic efficiency, $C_L/(C_D+C_E)$
η_R	=	spanwise location of the center of pressure, origin at tunnel wall, C_R/C_N
ν	=	kinematic viscosity
ρ	=	air density
Φ	=	phase angle between input signals to each actuator
χ_M	=	streamwise location of the center of pressure, origin at midchord, C_M/C_N
Ω	=	dimensionless vorticity, $(\partial v/\partial x - \partial u/\partial y)/U_\infty c$

Presented as Paper 2002-3270 at the AIAA 1st Flow Control Conference, St. Louis, MO, June 2002; received 7 December 2003; revision received 31 March 2004; accepted for publication 1 April 2004.

*Graduate Student, Department of Fluid Mechanics and Heat Transfer, Faculty of Engineering.

†Research Associate, Department of Fluid Mechanics and Heat Transfer, Faculty of Engineering; currently Resident Research Associate, National Research Council, NASA Langley Research Center, Hampton, VA. Senior Member AIAA.

‡Senior Lecturer, Department of Fluid Mechanics and Heat Transfer, Faculty of Engineering. Associate Fellow AIAA.

§Professor, Department of Fluid Mechanics and Heat Transfer, Faculty of Engineering; also AME Department, University of Arizona, Tucson, AZ.

I. Introduction

THE flow over a thin delta wing that is inclined to the freestream at high incidence angles separates at the leading edge and forms shear layers that roll up into two large vortices, which are primarily responsible for the lift generation at low speeds. These vortices are only weakly dependent on Reynolds number whenever the leading

edge is sharp.[1] As the incidence angle increases, the swirl velocity and the circulation of the vortices also increases. When the ratio of swirling-velocity-to-axial-velocity at any point in the vortex exceeds approximately 1.3, the vortex breaks down, that is, it expands into a highly fluctuating structure in which the velocity components are drastically reduced in the central part of the structure.[1] Consequently, vortex breakdown is generally associated with delta wing stall and can induce vibrations and buffet,[2] loss of control, and eventually wing damage.

The need for high lift during landing approach and low-speed maneuvers has been traditionally overcome by means of leading-edge slats and flaps[3,4] and multi-element high-lift systems.[5,6] However, the need to reduce weight and complexity has motivated numerous active flow control studies, involving steady blowing in particular, for example, from the trailing edge,[7,8] along the span,[9,10] and along the vortex core.[11] Significantly greater reductions in weight and complexity can be achieved with autonomous zero-mass-flux actuators.[12] However, their utility in delaying vortex breakdown and enhancing delta wing performance is, as yet, unproven.

Leading-edge vortices can conceivably be viewed as rolled up, or curved, shear layers possessing axial flow, and it is well known that two-dimensional free shear layers are particularly receptive to periodic excitation.[13] Indeed, it was shown that excitation along the leading-edge of a 60-deg swept delta wing significantly affected the evolution of the bound shear layer originating from the leading edge.[14] Similar observations demonstrated the effect by means of large flap oscillations, at prevortex breakdown conditions.[15–18] Periodic excitation apparently introduces "instability driven large eddies which periodically transport high momentum fluid to the surface"[19] and increased the poststall normal force on the wing.[20] On the other hand, excitation did not affect the prestall lift and drag forces,[21] supporting the notion that a mechanism similar to a two-dimensional shear layer mixing enhancement is at work. Roll control was achieved through microelectromechanical systems devices acting on a round leading edge[22] by altering the mean location of the separation line at the leading edge and, thus, the moment acting on the wing.

The underlying mechanism of performance enhancement by periodic excitation on a delta wing is unclear, with speculations ranging from delay of vortex breakdown to vortex enhancement. It was suggested[23] that vortex breakdown could be delayed by about 25% of the chord by introducing periodic perturbations at the leading edge. In contrast, water-tunnel particle image velocimetry (PIV) data[24] suggest that the vortex breakdown location was not altered, but that the downstream-directed velocity close to the surface increased, thereby decreasing the upper surface pressure. A follow-up study[25] ascertained that excitation from the aft-half of the leading edge, in the vicinity of the vortex breakdown location was most effective. PIV measurements revealed that the shear layer transports high streamwise momentum fluid into the wake, downstream of the breakdown location.

The aforementioned studies were exploratory in nature and did not directly measure the effect of leading-edge excitation on aerodynamic forces and moments. Furthermore, there is no obvious indication as to the optimum reduced frequencies, for example, $F^+ = 5.5$ (Ref. 14) or $F^+ = 1.2$–1.75 (Refs. 19, 20, and 23–25). Although there is consensus that excitation increases $C_{L\max}$ by maintaining a positive lift slope at higher incidence angles, it is not clear whether vortex breakdown is delayed[19,20,23] or whether major effects occur downstream of the breakdown that enhance the streamwise axial velocity.[24,25]

The main objective of this investigation was to determine the flow control conditions for which delta wing performance is optimally enhanced. This was achieved by conducting a parametric study on a balance-mounted semispan delta wing on which the effects of reduced frequency, perturbation amplitude, waveform, and phase were considered. An array of five autonomous piezoelectric actuators, mounted along the leading edge of the wing, was employed for this purpose. Balance data was supplemented by limited upper surface pressure measurements, and optimum control conditions were further investigated by two-dimensional PIV measurements in a plane that was normal to the root chord of the wing.

II. Experimental Setup

A. Delta Wing Model and Measurements

Experiments were performed on a semispan delta wing model with a 350-mm root chord, a 60-deg sweep angle Λ, a sharp leading edge, and a 5.7% thickness-to-root-chord ratio (Figs. 1a and 1b). The leading edge was beveled at 23 deg and 11 deg on the upper and lower surfaces, respectively. The wing included 5 internal piezoelectric actuators and was equipped with 10 upper surface pressure taps along a line perpendicular to the leading-edge at $x'/c' = 0.7$ (Fig. 1a). Pressure measurements were made with a scanning system connected to a 10-mm-Hg pressure transducer, with an uncertainty of $\pm 0.06\%$. For convenience, two different coordinate systems were employed, and these are defined in Fig. 1a.

The semispan wing was mounted on a four-component balance adjacent to the sidewall of a low-turbulence, closed-loop wind tunnel, with test section dimensions 609 (width) by 915 mm (height). The balance measured normal and tangential forces, as well as pitching moment about midchord and rolling moment about root chord (origin of χ_M and η_R in Fig. 1a). Uncertainties associated with the balance, as well as experimental parameters, are presented in Table 1.

Table 1 Parameters ranges and associated experimental uncertainties

Parameter	Uncertainty	Range
Temperature, °C	0.1	16–26
Re	2%	1.17–3.50×10^5
F^+	2%	0–10
α, deg	0.2	25–45
Excitation Voltage	1%	0–80 V
Input power	2%	0–2.5 W
C_μ	25%	0–3.8%
Force balance		
C_N		0.1–7
$Re = 1.17 \times 10^5$	0.08	
$Re = 2.34 \times 10^5$	0.043	
$Re = 3.50 \times 10^5$	0.015	
C_M		−0.15–0
$Re = 1.17 \times 10^5$	0.007	
$Re = 2.34 \times 10^5$	0.004	
$Re = 3.50 \times 10^5$	0.002	
C_R		–0.04–0.34
$Re = 1.17 \times 10^5$	0.015	
$Re = 2.34 \times 10^5$	0.013	
$Re = 3.50 \times 10^5$	0.006	

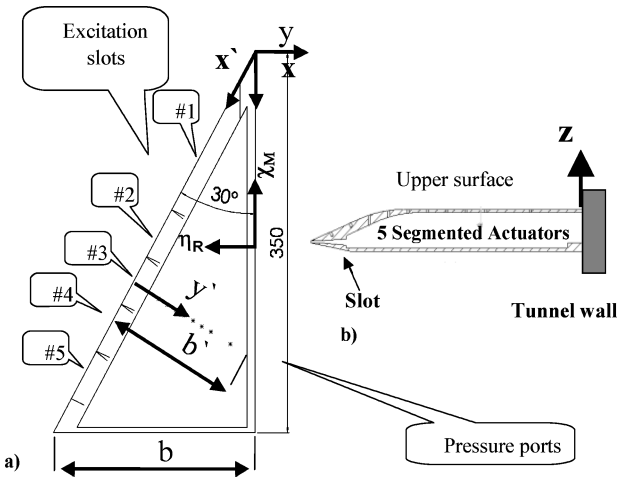

Fig. 1 Semispan delta wing model: a) top view and b) wing's cross section.

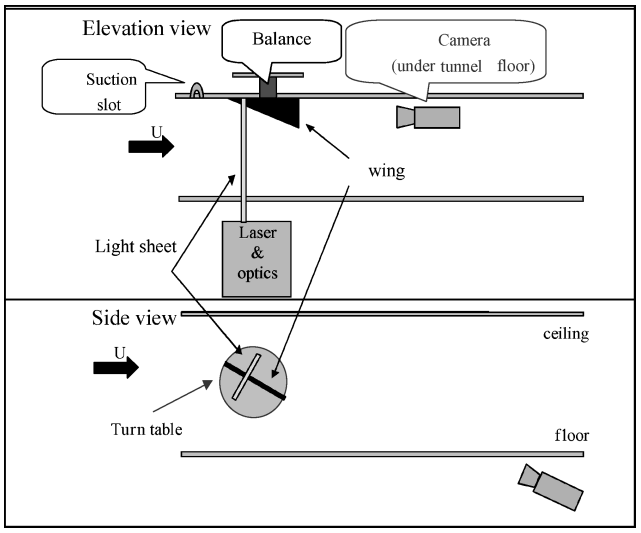

Fig. 2 Schematic wind tunnel and PIV setup.

The tests were conducted at speeds of 5–15 m/s, corresponding to root chord Reynolds numbers of $1.2–3.6 \times 10^5$.

The tunnel wall boundary layer upstream of the wing was removed by means of suction applied through a porous strip, located 25 cm upstream of the wing apex, showing a negligible effect on the forces and moments generated by the semispan model.

The zero-mass-flux piezoelectric actuators were segmented and distributed evenly along the leading edge (LE) of the wing. Each actuator cavity was connected to an exit slot via a slightly convergent nozzle (Fig. 1b). The actuators' locations correspond to slots 1 (close to the apex) through slot 5 (close to the wing tip), as shown in Fig. 1a. Slot segments were 1 mm wide and spanned approximately 12% of the LE length, apart from the slot closest to the apex, that is, slot 1, which spanned 34% of the LE length, with its upstream edge located at 8% from the apex. The actuators were driven by a multiple-wave function generator, via a five-channel amplifier. A comprehensive bench-top calibration was performed before and after the wind-tunnel runs to characterize and verify each actuator's output and determine C_μ. This included relevant frequency and amplitude sweeps, as well as amplitude modulation and burst modes.

Baseline and controlled flowfields perpendicular to the wing surface and wind-tunnel wall were measured with a two-component PIV system, using a double-pulsed Nd–Yag laser, and a cross-correlation charge-coupled device camera, with a 1300×1030 pixel resolution. (See Fig. 2 for a schematic of the setup.) The camera was mounted underneath the tunnel floor, in which a small square opening was made to obtain a distortion-free optical path. Seeding was provided by a theatrical fog generator located upstream of the test section.

B. Modes of Excitation: Definitions

The actuators were operated in three modes: 1) by a pure sine wave, 2) by an amplitude modulated sine wave, and 3) by a burst mode.[26,27] Additional modulation techniques or envelope shapes were considered (Sec. III.C), but not studied in detail.[28] Figures 3a–3c show examples of the three modes, where the function generator (input voltage) signal is shown together with the derectified hot-wire measured velocities. Mode (1) is self-explanatory. For amplitude modulation (AM, mode 2), the amplitude of the carrier wave is modulated by the modulating wave. The carrier wave has a frequency of $f_r = 1/T_r = \omega/2\pi$, and the modulating waves' frequency is $f_m = 1/T_m$, which is an integer divisor thereof. For burst mode (BM, mode 3), the carrier amplitude is modulated by a square wave having an amplitude that varies between 0 and 1, and its overall duration for n cycles is nT_r. The square wave modulating frequency is f_m. Therefore, in addition to the preceding definitions, we can also define a duty cycle (DCy) $= nT_r/T_m$ (alternatively, nf_m/f_r), which expresses the fraction of the cycle during which the actuators are active. Consequently, in BM, C_μ is also a function of DCy (and not only of the peak excitation voltage, to be discussed). Note that for the AM and BM, the reduced excitation frequency F^+ is based on f_m.

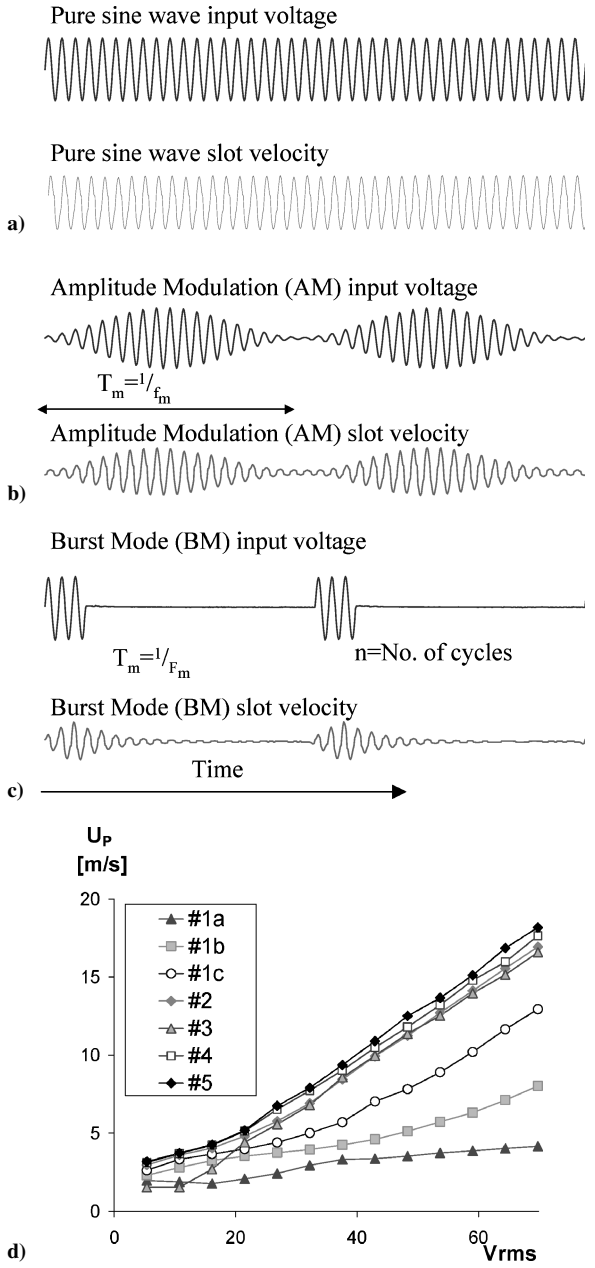

Fig. 3 Response of a hot wire placed at the excitation slot to different modes: a) pure sine wave, b) AM, c) BM and d) bench-top slot calibration with pure sine excitation at 1170 Hz.

The spectral content of the AM waveform (corresponding to the signal shown in Fig. 3b) is characterized by a major amplitude peak at f_r and two minor peaks at equal distance on each side of this point $f_r \pm f_m$. The BM waveform results in a more dispersed spectrum, containing peaks at constant f_m increments from each other. The amplitude of these peaks is constrained by a function similar to $[\sin(x - f_r)]/(x - f_r)$ (Ref. 29). The higher the DCy is, the higher the energy that is concentrated around f_r.

C. Slot Calibrations and Definitions

The excitation amplitude coefficient is defined[30,31] as

$$C_\mu = \frac{\sum_{i=1}^{K} \rho u_i'^2 A_i}{\frac{1}{2}\rho U_\infty^2 A_w}$$

Because of hot-wire limitations at resolving low-speed velocities, each actuator's characterization was based on peak exit slot

velocities U_{Pi} and assumed to be sinusoidal, resulting in $U_{Pi}^2 = 2u_i'^2$, where u_i' is the rms of velocity fluctuations at the slot exit.

A bench-top calibration was performed to evaluate the fluidic output of the actuators. A hot wire was placed in the core region of each slot, and the exit slot velocity was measured for a series of excitation levels (Fig. 3a) at the actuator's resonance frequency. Additional data were acquired to characterize the fluidic output when applying AM and BM voltage excitation signals at $f_m \leq 146$ Hz (corresponding to $F^+ \leq 5$ at $Re = 2.34 \times 10^5$), and all data were compared to that at 58.5 Hz (corresponding to $F^+ = 2$ at $Re = 2.34 \times 10^5$). The measured 58.5-Hz AM signal closely followed the voltage input as shown in Figs. 3b. However, the momentum output was slightly reduced (typically by less than 20%) when compared with the ideal excitation signal, due to the actuator exponential rise time. Consequently, all C_μ were based on the ideal behavior of the waveform, and the uncertainty was estimated at ±25%. The rise-time effect was greatly exacerbated when applying the BM signal and this was particularly evident at low DCy. Consequently, C_μ calibration was based on the measured velocity signal. Hot-wire traverses across the span and width of the slot revealed small variations (less than 6%) in C_μ.

Following the traditional analysis of swept LEs, we consider the LE normal velocity component $U_\infty \cos\Lambda$ and the component of the chord normal to the LE, namely, $c\cos\Lambda$, which is the effective maximum length scale. Substituting these two quantities into the traditional definition of F^+ results in $F^+ = fc/U_\infty$, which is appropriate to the delta wing and, therefore, used throughout this paper.

A typical actuators' characterization curve showing peak exit slot velocities U_P as a function of the rms excitation voltage V_{rms} at $f = 1170$ Hz is shown in Fig. 3d. Figure 3d presents velocities normal to the slot, within the slot-exit core region. The peak velocities emanating from slots 2–5 are similar and increase almost linearly with V_{rms}. However, three measurements at different locations along slot 1 show decreasing peak velocities toward the apex (Fig. 3d). This is because the larger cavity volume, adjoining slot 1, as well as the slot span and possible viscous effects. Note, however, that the normal component of momentum generated at slot 1, that is, $\rho U_{p1}^2 A_1$, was about 80% of that generated by each of the other slots.

Performance validation of the actuators following the termination of the wind-tunnel experiments revealed a significant performance degradation of actuators 1, 2, and 3. Consequently the C_μ values quoted here (based on the initial calibration made before the commencement of the data acquisition) should be considered as upper bound of the actuators' performance. The parameter ranges and associated experimental uncertainties are presented in Table 1. The uncertainty of the balance data was evaluated using a three step procedure:

1) The difference between tare measurements performed before and after each baseline polar, that is, varying α.

2) For every α, the standard deviation of all of the baseline data (multiplied by 3).

3) For the controlled data acquired at fixed α, a baseline was taken at the beginning and at the end of each parameter scan.

The uncertainty of the PIV data is 0.3 m/s (or 3%) at $x/c = 0.25$ and 0.8 m/s (or 8%) at $x/c = 0.6$.

III. Discussion of Results

A. Effects of Excitation Frequency, Amplitude, and Waveform

Stall occurs naturally on the present wing at $31 \leq \alpha \leq 32$ deg and is insensitive to Reynolds number (Fig. 4a), generating a maximum normal force of $C_{N,\max} \approx 1.32$–1.37 in the range of Reynold numbers tested. Stall is mild where the normal force decreases by about 0.015/deg (for $\alpha < 40$ deg) followed by a normal force plateau (for $40 < \alpha < 45$ deg). During the exploratory stage of the investigation, the wing was held at a constant poststall angle of attack. The data presented in Fig. 4b were acquired at $\alpha = 37.8$ deg and show the dependence of the normal force on F^+, where AM was used to obtain $0 \leq F^+ \leq 10$ at a constant $C_\mu = 0.41\%$, for three Reynolds numbers. The force increment resulting from the excitation was mostly dependent on F^+ with only a weak sensitivity to the Reynolds number (with the exception of the lowest Reynolds number tested and where $2 \leq F^+ \leq 6$), showing a peak normal force increment of $\Delta C_N / C_N \approx 15\%$. This peak is more pronounced at the higher Reynolds numbers using $1 < F^+ < 2$, whereas at the lowest Reynolds number Re, there is a larger range of effective frequencies, that is, $1 \leq F^+ \leq 4$. Note that for $F^+ > 8$, excitation can have a deleterious effect on the performance. These observations are consistent with published data,[14,19,20,24,25] despite the fact that an AM signal was used presently to generate the low F^+. This is probably because the flow is not receptive to the carrier frequency.[26] To further illustrate this point, note that pure sine-wave excitation at the carrier frequency, which is in the range $27 \leq F^+ \leq 82$ (depending on Reynolds number Re), has a negligible to slightly detrimental effect on C_N (circled data points in Fig. 4b).

The effective F^+ and accompanying C_μ, obtained in various investigations at relatively low and intermediate Reynolds numbers are illustrated in Table 2. They all indicate that the optimum reduced frequency to be used is of order unity.

In additional experiments, it was found that excitation reduces the nose-down pitching moment C_M when the most effective reduced

Table 2 Summary of effective F^+ and C_μ from various investigations

Reference	Effective F^+	C_μ, %	$Re \times 10^4$
Gad-el-Hak and Blackwelder[14]	5.5	0.3–1.28	1.25
Gu et al.[15]	1.3	7.7[a]	1.7
Guy et al.,[19,20,23] Siegel et al.[24,25]	1.2–1.75	1.9–2.3[a]	2.1–55
Present investigation	1.0–4.0	0.41, 3.8	11.7
Present investigation	1.0–2.0	0.03–0.41	23.5–35.0

[a]Calculated according to the definitions presented in this study (see Nomenclature).

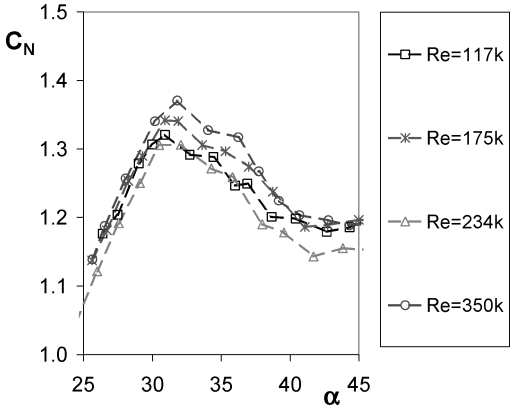

Fig. 4a Reynolds number effect on baseline C_N.

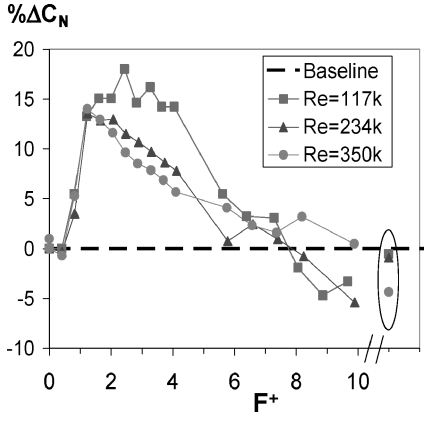

Fig. 4b Frequency effect on ΔC_N at $\alpha = 37.8$; excitation AM, $C_\mu = 0.4\%$; circled points $F^+ = 82$, 41, and 27 (corresponding to $Re = 1.17$, 2.34 and 3.50×10^5). $C_\mu = 0.29\%$ for the pure sine excitation.

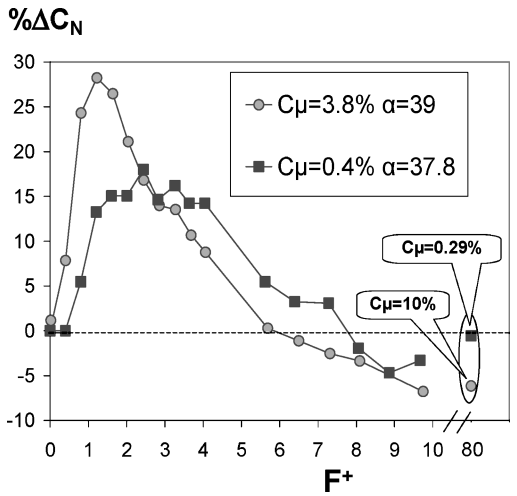

Fig. 5 Frequency effect on ΔC_N using low and high C_μ; $Re = 1.17 \times 10^5$, AM excitation; encircled points pure sine, $F^+ = 82$.

frequencies are used. Furthermore, the longitudinal center of pressure varies by no more than 2% of the chord as a consequence of the excitation. The positive movement of the center of pressure at effective F^+ implies that the normal force was increased at the front-half of the wing slightly more than at its rear-half. These findings suggest that the C_N enhancements (Fig. 4b) are not brought about by a dramatic change in the vortex dynamics along the wing, but rather an almost uniform mixing enhancement across the separating shear layer from the sharp LE (as will be shown and discussed later). In contrast to C_M, C_R is strongly dependent on the frequency, that is, a variation of $\Delta C_R \approx 0.06$ between $F^+ = 1$ and 10. Furthermore, the transverse location of the center of pressure was not affected by the excitation, irrespective of the frequency or the momentum input. This would indicate that, in a time-mean sense, the vortex did not move in a direction normal to the leading edge.

Frequency scans using AM at two values of C_μ, differing by an order of magnitude, at similar angles of attack are shown in Fig. 5. The 10 fold increase in C_μ slightly reduces the optimal F^+ as well as narrows the effective F^+ range. Nevertheless, the relative increase in the normal force ΔC_N is approximately doubled. Similar qualitative observations have been made on airfoils, namely, that large increases in C_μ bring about modest performance enhancements.[32,33] At high C_μ, lower $F^+(<3)$ achieves better performance, yet the effective F^+ range becomes narrower. The improved performance at lower F^+ with higher C_μ is consistent with previous observations made in several two-dimensional flows.[32–34] On the other hand, the narrowing of the effective range of F^+ contradicts those observations and requires further study.

The effect of modulation envelope shapes (shown in Fig. 6a) on ΔC_N is shown in Figs. 6c, where the calibrated C_μ was maintained constant for all cases. The spectral content of the derectified velocity at the excitation slot is shown in Fig. 6b. In general, the "chainsaw" and BM envelopes were somewhat superior to the "triangle" and AM envelopes, with regard to C_N enhancement, for the range of effective frequencies considered. Also the hot-wire response measured in the slot for the two effective excitation signals was similar (Fig. 3c). Note that the most effective waveform, that is, chainsaw, had the largest number of harmonics of the modulation frequency f_m (Fig. 6b). It appears that the shorter the excitation rise time, the larger is the improvement in C_N. The wider spectral content of some of the excitation waveforms (Fig. 6b) may have enabled a more effective amplification of the most unstable modes of the separated shear layer and promoted a nonlinear interaction among a wider spectrum of excited waves. Consequently, a detailed comparison between AM and BM excitation modes at various frequencies was carried out, and the results are shown in Figs. 7a and 7b, where peak excitation voltage was maintained constant. For AM excitation, this corresponded to $C_\mu = 0.4\%$ for all F^+, but for the BM excitation C_μ

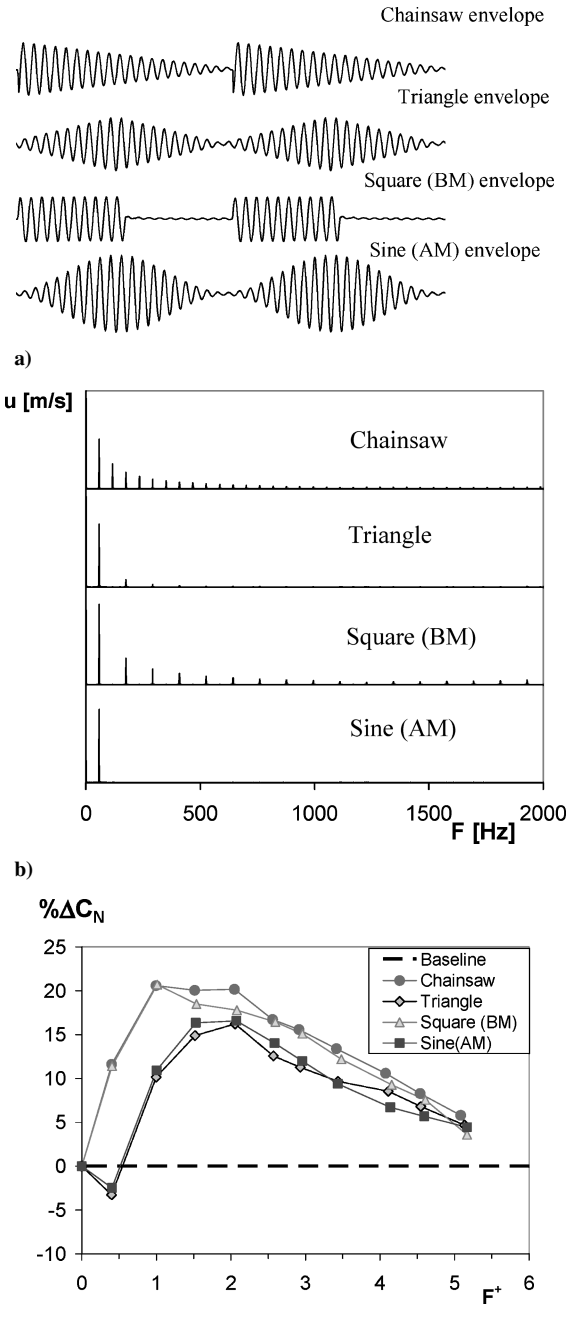

Fig. 6 Effect of modulating envelope shape on the frequency response. $Re = 2.34 \times 10^5$, $\alpha = 37.8$ deg, $C_\mu = 0.4\%$: a) waveforms, b) fast Fourier transform of the absolute value of the velocity output of each waveform, and c) ΔC_N.

increased in proportion to the DCy and the latter increased with increasing F^+. This is because the number of BM active cycles, $n = 3$ remained constant, whereas the number of cycles between bursts decreased as F^+ increased. To further illustrate this, selected BM C_μ values are shown in Fig. 7a, with the ordinate on the right-hand side. The data presented in Fig. 7a indicate that BM excitation is superior to AM excitation in enhancing C_N for the entire F^+ range considered and that its low F^+ threshold of effective frequency range is roughly half that of the AM. In addition, BM excitation brings about higher normal force enhancement using significantly lower C_μ. For example, at $F^+ = 0.4$, AM slightly degrades performance, whereas BM enhances it, even with 29 times lesser C_μ. Similarly, at $F^+ = 1.0$, the normal force enhancement using BM is doubled when using 11 times smaller C_μ than for AM. Consequently, the quotient $\Delta C_N / C_\mu$ can be up to three orders of magnitude larger for BM than for AM (Fig. 7b), suggesting perhaps that the use of a

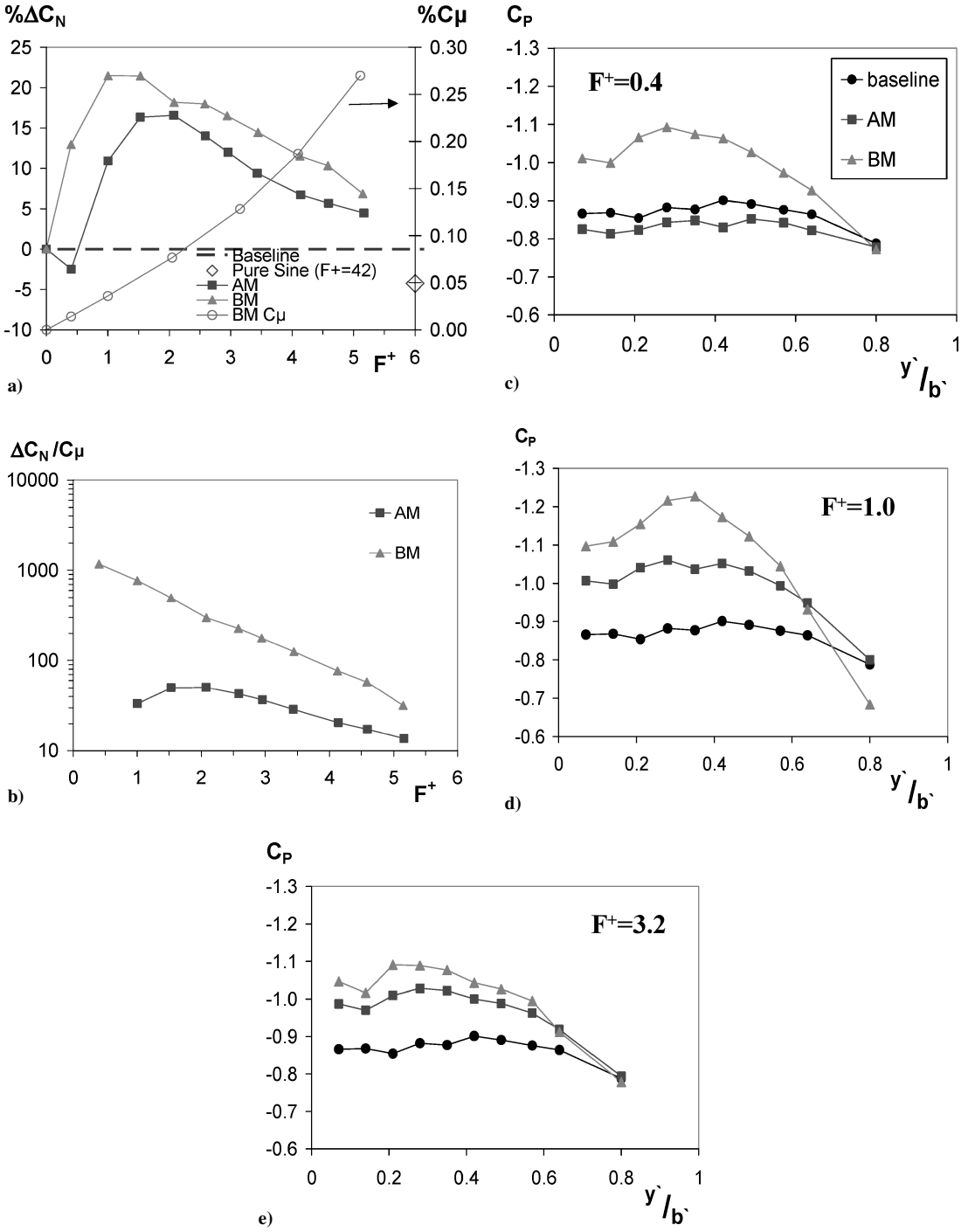

Fig. 7 Frequency effect on performance $\alpha = 37.8$ deg, $Re = 2.34 \times 10^5$, AM excitation of $U_P/U_\infty = 1.3$ and BM of $U_P/U_\infty = 0.83$ (note the log scale on the ordinate): using low C_μ a) ΔC_n and b) $\Delta C_n/C_\mu$ and frequency effect on C_p at low C_μ, pressure ports at $x'/c' = 0.7$: c) $F^+ = 0.4$, d) $F^+ = 1.0$, and e) $F^+ = 3.2$.

single parameter describing the amplitude of the excitation, such as C_μ, is not adequate. Pressure distributions, measured normal to the LE at $x/c = 0.7$ for $F^+ = 0.4$, 1.0, and 3.2 (Figs. 7c–7e), provide a qualitative validation of the balance data and offer some insight into the structure of the flow in the plane of the measurement. The baseline's approximately constant pressure distribution implies a detached flow without the presence of a vortex. Using $F^+ = 0.4$, the slight degradation due to the AM and the performance enhancement due to the BM are qualitatively reflected by the upper surface pressures (Fig. 7c). Furthermore, the discernable C_P peak at $y/b = 0.3$, associated with the BM excitation, suggests the existence of a diffused vortical structure at this cross section. When $F^+ = 1$ is used, the peak suction pressure generated by BM excitation (Fig. 7d) is clearer than for the AM, and it remains centered around $y/b = 0.3$. In contrast, the pressure distribution associated with AM does not resemble a clear vortex signature and is approximately constant over the range $0.1 \leq y/b \leq 0.6$. Finally, when $F^+ = 3.2$ (Fig. 7e) is used, both controlled pressure distributions have a similar shape, whereas the lower overall pressure is still associated with the BM excitation. Frequency scans conducted at different angles of attack indicated similar trends to those shown in Figs. 7.

B. Effects of AM Excitation Amplitude

Figures 8a–8d present the ΔC_N and C_P data resulting from C_μ scans at a constant F^+, that is, changing the modulation amplitude in AM mode. The variation of the normal force with amplitude

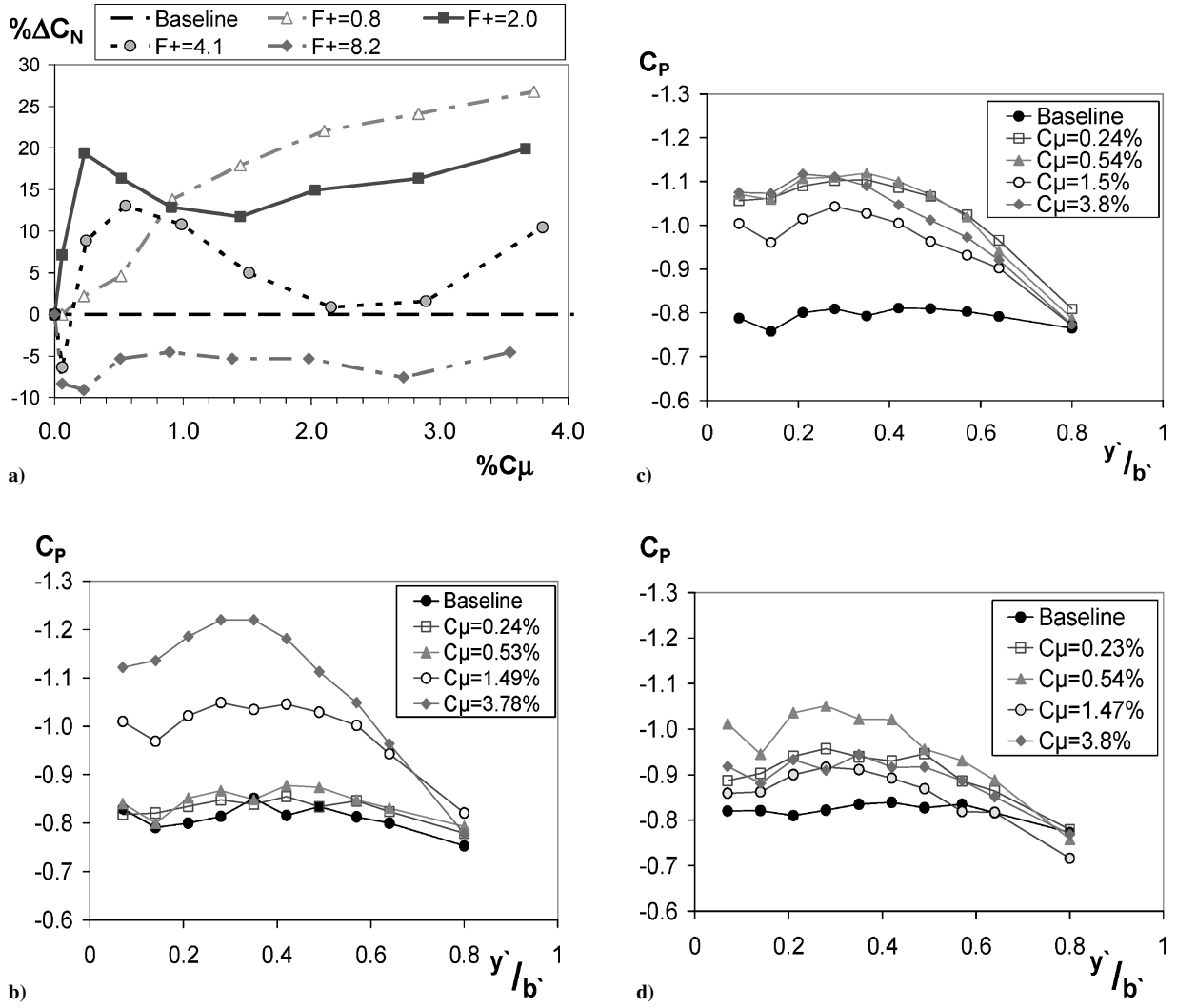

Fig. 8 C_μ effect using AM excitation, wing at $\alpha = 37.8$ deg, $Re = 1.17 \times 10^5$: a) normal force variation, and pressure measured at $x'/c' = 0.7$ pressure distribution C_p, b) $F^+ = 0.8$. c) $F^+ = 2.0$, and d) $F^+ = 4.1$.

changes significantly for different AM frequencies. For example, at a low frequency of $F^+ = 0.8$, C_N continuously increases (although not at a fixed rate), with increasing C_μ. On the other hand, at $F^+ = 2.0$, there exists an optimum at $C_\mu \approx 0.4\%$. Further increase in C_μ brought about a slight reduction in ΔC_N, followed by a gradual C_N increase for $C_\mu > 1.5\%$. At higher $F^+ (= 4.1)$, a similar trend is evident, with a local maximum around $C_\mu \approx 0.5\%$ that degenerated to nullify ΔC_N at $C_\mu \approx 2\%$, but regained some effectiveness for $C_\mu > 3\%$. At even higher frequencies ($F^+ = 8$), the effect of AM excitation is deleterious irrespective of C_μ. When possible applications are considered, the continuous rise of ΔC_N due to excitation at $F^+ = 0.8$, and especially the roughly linear response when $C_\mu > 1.0\%$, makes this reduced frequency perhaps amenable to autonomous closed-loop control despite that it would not be the most efficient frequency to use under all circumstances.

The C_N performance variations shown in Fig. 8a are in qualitative agreement with the variations of the pressure distributions shown in Figs. 8b, 8c, and 8d (for $F^+ \approx 0.8$, 2.0, and 4.1, respectively). The local minima exhibited by C_N, as a result of increasing C_μ at $F^+ \geq 2$, is counterintuitive in the context of conventional active flow control (AFC) wisdom. However, note that similar observations have been made on two-dimensional airfoils.[32,33] This similarity, together with the optimum F^+ ($\approx$1), suggests that the shear layer forming the vortex on a delta wing has some resemblance to the classical, excited mixing layer between two parallel streams and the two-dimensional separated zone.[13,31,34]

C. BM Amplitude–C_μ Dependence

A comparison of ΔC_N generated by AM and BM excitation modes at various values of C_μ is shown in Fig. 9 for $F^+ = 2.0$, at a poststall incidence of $\alpha = 37.8$ deg (Note that the C_μ is plotted on a log-scale.) For BM actuation, data for various fixed DCys are presented. Note that the BM C_μ can be increased when altering either U_p or DCy; here, U_p was increased for each DCy presented. AM excitation at low C_μ has a very weak effect on the normal force, and discernable effects are only evident at AM $C_\mu > 0.1\%$. Further increase of the AM C_μ results in a maximum ΔC_N that is achieved at $C_\mu \approx 0.4\%$, whereas additional increase in C_μ results in performance degradation. In contrast, BM excitation with a small DCy = 5% has a measurable effect on ΔC_N corresponding to a BM C_μ that is as low as 0.001%, that is, two orders of magnitude smaller than for AM excitation. This particular DCy (5%) comprises a single excitation cycle out of a total of 20, corresponding to a DCy = 100%. Increases in U_p result in logarithmic increases in C_N with saturation at $C_\mu > 0.02\%$. At low C_μ ($\approx$0.01%), increasing DCy results in slightly smaller C_N enhancement. This is an important observation because it means that, at low C_μ, the lowest DCy, that is, $n = 1$, can be used to achieve significant gains. This outstanding result could perhaps be explained by the fact that a short, strong impulse (delta function) contains a complete spectrum of excitation modes. Hence, the separated shear layer is supplied with a wide range of frequencies, from which the most unstable ones can be amplified and, thus, generate large coherent structures. It was shown that the timescales associated with a change of state of the flow (from being separated to

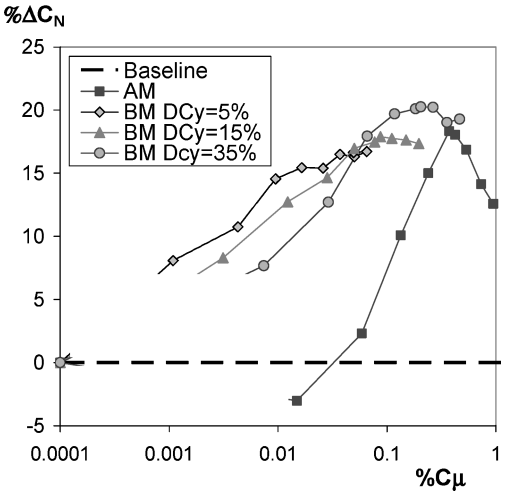

Fig. 9 Effect of the excitation C_μ on normal force variation: C_μ altered by changing the peak slot exit velocity, U_p, $\alpha = 37.8$ deg, $Re = 2.34 \times 10^5$, $F^+ = 2.0$, baseline shown for $C_\mu = 0.0001\%$.

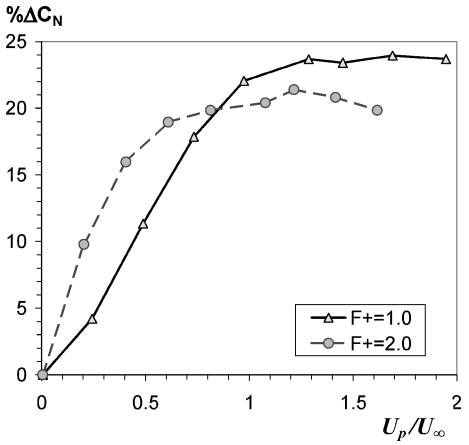

Fig. 10 Effect of the excitation peak exit slot velocity on C_N increment, $\alpha = 37.8$ deg, $Re = 2.34 \times 10^5$, BM excitation, DCy = 20%.

being attached and vice versa) are much longer than the timescales of the excitation.[35] Therefore, if a single pulse is able to attach the flow or sufficiently change its characteristics, it will remain at the modified state for a considerable time thereafter. These results also raised the question of whether C_μ is the adequate parameter to describe the excitation's magnitude. This matter will be discussed in the following section. For progressively larger DCys, larger ΔC_N can be affected, but at successively larger values of C_μ. Nevertheless, applying BM excitation at DCy = 35% and $C_\mu = 0.08\%$ produced a ΔC_N peak that was larger than the peak generated by the AM excitation at the five times larger C_μ (≈0.4%).

Figure 10 shows a comparison between the effects of BM excitation using $F^+ = 1.0$ and 2.0 on the normal force increment. Here also, the DCy was held constant and the peak slot exit velocity was altered to increase the excitation C_μ. Note that the abscissa is the normalized peak slot exit velocity and not C_μ. The higher frequency, that is, $F^+ = 2.0$, is more effective at low amplitudes, but it saturates for U_p of 70% the freestream velocity, whereas the lower frequency, $F^+ = 1.0$, becomes superior only at $U_p/U_\infty > 0.8$ and provides a slightly higher normal force increment, and saturates at $U_p/U_\infty \approx 1.2$. When both the peak velocity and momentum coefficient are considered, it could be stated that it is most efficient to use peak velocities between 50 and 80% of the freestream and momentum coefficients smaller than 0.2%.

Also note that the slot exit velocity did not reach the steady-state response to applied voltage excitation for $n \leq 4$ cycles, compared to $n = 3$ in Fig. 3c. As the number of cycles is increased, a critical DCy is reached, above which performance degradation is evident. This

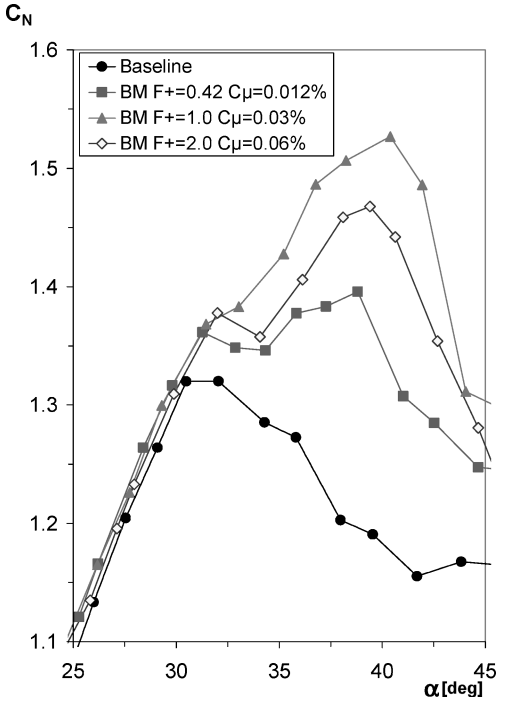

Fig. 11 C_N vs α for BM excitation at various F^+; $Re = 2.34 \times 10^5$, BM excitation, $n = 3$ cycles, $U_p/U_\infty = 0.7$.

critical DCy appears to be, in most cases, larger at higher slot-peak velocities. The degradation in performance at large DCy (≥35%) could be explained perhaps by observing that the slot exit velocity does not decay immediately after the termination of the excitation signal, but it persists for several additional cycles (Fig. 3c) due to inertia or cavity resonance, leading to a larger effective DCy. This in turn causes the BM to resemble a pure sine-wave excitation, losing the low-frequency content and consequently losing efficiency.

The most important observation that can be drawn from this section is that the results are virtually independent of the DCy, even though it was increased sevenfold and more (from 5 to 35% and more). This finding might lead to reconsideration of C_μ, based on the fractional duration of the excitation in BM excitation, as the leading magnitude parameter for this excitation mode and flow regime.

D. Angle-of-Attack Variation with BM Excitation

After effective parameter ranges at a given incidence were established, the dependence of the normal force on the angle of attack was considered (Fig. 11). All of the curves in Fig. 11 were obtained using BM excitation at various F^+ where U_p and n were maintained constant. As with earlier two-dimensional investigations, excitation did not influence the flow at prestall incidence angles. The most significant effect of AFC was apparent at 7–10 deg beyond the baseline stall angle. Note, however, the kink in the C_N–α slope just beyond the baseline stall angle that is most apparent at reduced frequencies other than $F^+ = 1$. It is also evident that the lift slope associated with excitation is smaller in the poststall regime than the corresponding prestall slope. This suggests that the excitation generates vortices that are somewhat different in nature than the vortices existing over the unperturbed delta wing and will be further discussed in Sec. III.G.

E. Effect of Excitation Location

The effect of operating the actuators individually, thereby introducing the excitation only at selected locations along the LE, is shown in Figs. 12a and 12c and in Figs. 12b and 12d for AM and BM excitation modes, respectively. Note that for the AM excitation, only the two actuators closest to the apex increase C_N (Fig. 12a), whereas the remaining actuators closer to the trailing edge are deleterious, particularly actuator 4. In contrast, BM excitation is not as sensitive to the location of the active actuator (Figs. 12b), and all actuators

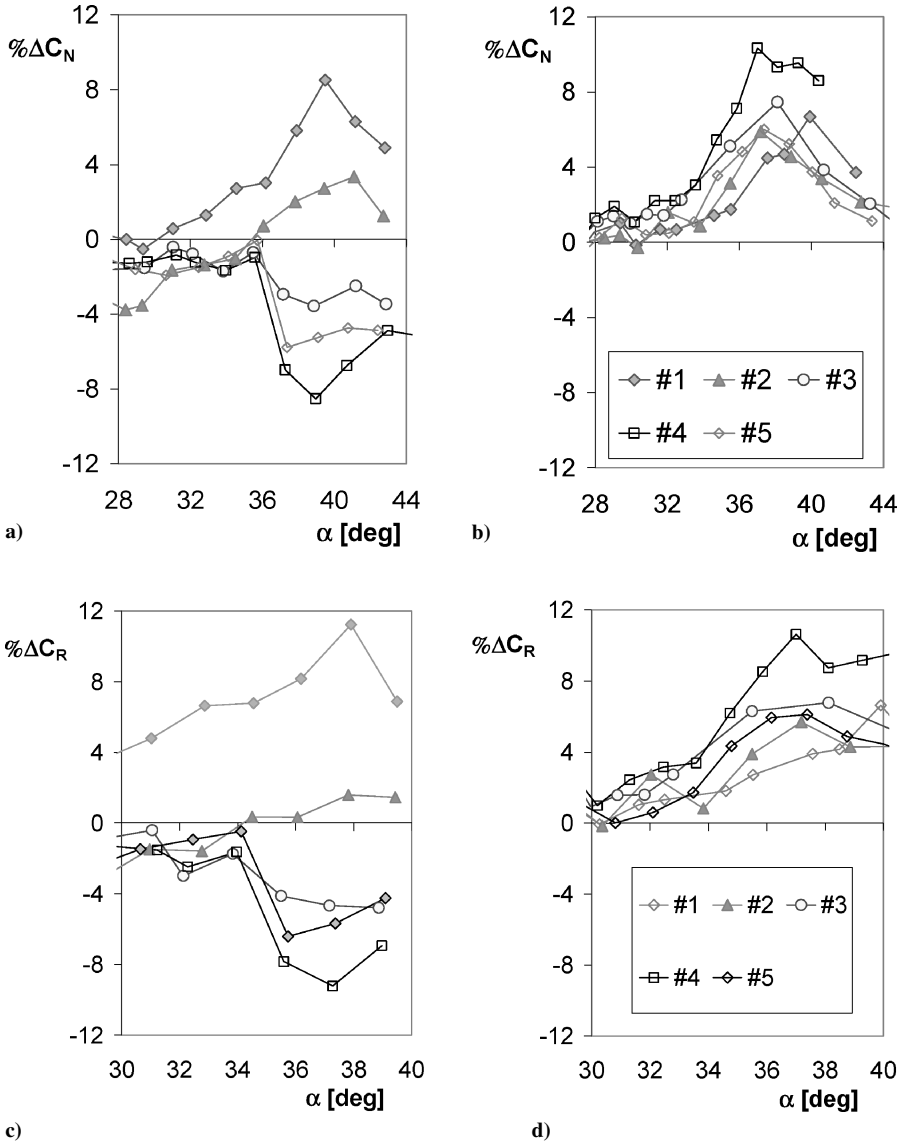

Fig. 12 Effect of active slot segment on performance, $Re = 2.34 \times 10^5$, AM excitation, $F^+ = 2.0$, $C_\mu = 0.19\%$; BM, $F^+ = 1.0$, $C_\mu = 0.006\%$, DCy = 7.5% (changes in % of baseline values): a) ΔC_N, AM, b) ΔC_N, BM, c) ΔC_R, AM, and d) ΔC_R, BM.

enhance C_N, with actuator 4 being slightly more effective than the others. The C_R data was consistent with the C_N trends and, thus, indicated the potential for rolling moment control (Figs. 12c and 12d). Rolling moment coefficients using AM excitation (Figs. 12c) generate either an increase or a decrease in rolling moment relative to the baseline, depending on the individual active slot location. For example, when slot 1 is active, C_R is increased, whereas C_R is decreased when slot 4 is active. These results could be most beneficial in future implementation of AFC for roll control. In contrast, BM excitation (Fig. 12d) brings about increased C_R irrespective of which slot is active, with slot 4 generating the largest ΔC_R produced by a single element operating in BM. In summary, with all actuators active (Secs. III.A–III.C), AM and BM actuation resulted in similar trends, where differences were mainly quantitative. In contrast, operating the actuators individually resulted in significantly different qualitative behavior. Exploration of the physical mechanism leading to these findings warrants further study.

F. Effect of Phase Variation Along the LE

Provided the effects of excitation are felt only downstream of the actuation, the alteration of the relative phase along the LE could affect the flow. This effect was investigated in an attempt to enhance the interaction between the excitation and the spiral vortex, provided that the flow is convectively unstable, amplifying the excitation emanating from individual slots.

Figure 13 shows the effect of operating each actuator at a phase-lag relative to its upstream neighbor, on the normal force, that is, the excitation is rendered successively less two-dimensional. Data are presented for the poststall incidence of $\alpha = 37.8$ deg, employing AM excitation at $F^+ = 2.0$. Several levels of C_μ were tested, but only one typical case is presented. It was found that performance is degraded as the excitation becomes less two-dimensional, with the exception of $\Phi = 30$ deg at $C_\mu = 0.4\%$. The most deleterious effects are evident in the vicinity of $\Phi = 180$ deg, that is, successive actuators are operated in antiphase. Despite this, at $C_\mu \geq 0.4\%$, the overall effect of actuation remains beneficial, but two-thirds of the C_N enhancement was lost. A more detailed phase-lag test was conducted for $C_\mu = 0.4\%$ and using a smaller $\Delta\Phi = 7.5$ deg. However, when C_N uncertainty was considered, this survey did not identify a more effective $\Delta\Phi$ that was other than zero.

The preceding discussion showed the utility of operating actuators individually. However, the most significant gains are achieved when all actuators are operating in unison at the same phase. This further reinforces the notion that the excitation does not bring about dramatic changes to the strength or breakdown location of the LE vortex. Rather, the separated shear layer along the entire LE is receptive to the excitation in a quasi-two-dimensional manner.

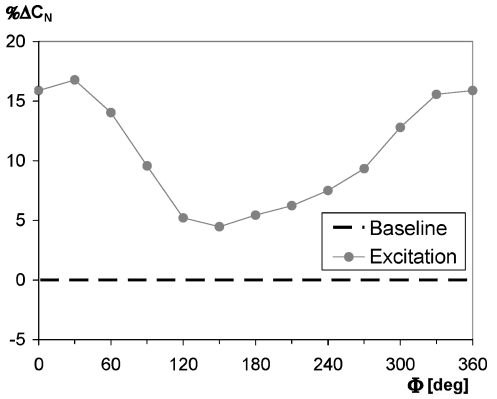

Fig. 13 Effect of phase lag between actuator segments on normal force increment; $Re = 2.34 \times 10^5$, $\alpha = 37.8$ deg, AM excitation, $F^+ = 2.0$, $C_\mu = 0.41\%$.

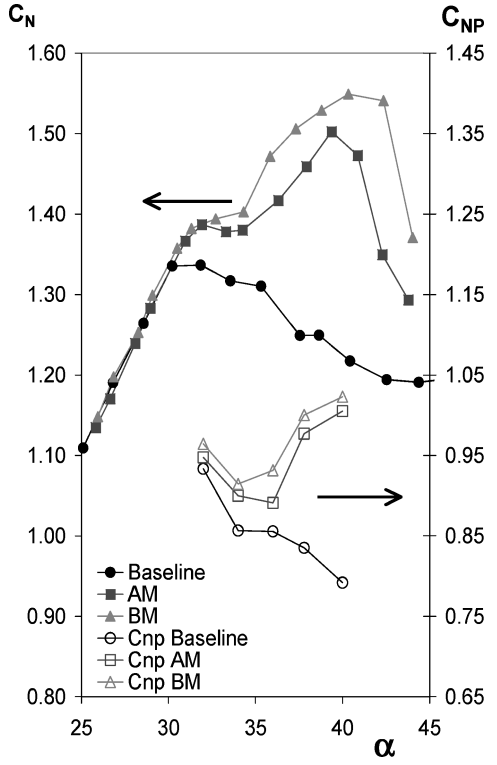

Fig. 14 Baseline and controlled normal force C_N and integrated $C_p(C_{NP})$ vs α; $Re = 2.34 \times 10^5$, AM excitation, $F^+ = 2.0$, $C_\mu = 0.41\%$; BM, $F^+ = 1.0$, $C_\mu = 0.03\%$, DCy = 7.5%. (C_{NP} ordinate is on the right side.)

G. Incidence Variation Under Optimal Excitation Conditions

Figure 14 shows normal force C_N and integrated pressure coefficient C_{NP} (right side ordinate) for the two excitation modes, at the maximum ΔC_N achieved by each of the excitation modes for low-momentum input defined here as $C_\mu < 0.5\%$. Corresponding to the baseline incipient stalled flow condition $\alpha = 32$ deg, both AM and BM excitation modes extend the linear C_N–α range by approximately 2 deg; thereafter, C_N remains approximately constant for $33 \le \alpha \le 34$ deg, in a manner similar to the incipient baseline stall (Fig. 14). However, for $\alpha > 34$ deg, both excitation modes bring about significant C_N enhancement, although $dC_N/d\alpha$ is somewhat lower than the prestall lift slope, except for the BM data at $\alpha = 35$–36 deg. This result is consistent with previous observations[23] that were based on the integration of upper surface pressures. This range of angles of attacks corresponds to a rapid decrease in $d\chi_M/d\alpha$, which indicates a change in the flow regime. As noted earlier (Figs. 6, 7, and 9), BM excitation is more effective in enhancing the normal force, despite the large disparity in the BM C_μ that is currently 13 times smaller than the AM C_μ. The C_P distribution at the incipient stall angle ($\alpha = 32$ deg, not shown) shows a distinct peak for baseline and excited cases at $y/b \approx 0.25$, where it is probably the footprint of the LE vortex. However, for both excitation modes at $\alpha = 36$ and 40 deg (not shown), the C_P peak is not as clearly defined and moves toward the wing root, although the pressure remains consistently lower than the baseline pressure. This finding illustrates that the C_N enhancement does not occur as a result of the classic, stationary LE vortex, and hence the poststall $dC_N/d\alpha$ is lower (Fig. 14), with the exception of $\alpha = 35$–36 deg BM data. It would appear that, on the average, the vortex is quite spread out in the spanwise direction. Because only mean pressures were acquired, it is not possible to distinguish if the vortex modified by the periodic excitation is narrower but meandering periodically in time, or if it is spread out, that is, diffused, and stationary. This observation, regarding the large mean width of the vortex is consistent with independent PIV measurements,[24] which show that the vortex center oscillates as a result of the excitation in an approximately elliptical orbit in the transverse (crossflow) plane.

Lift coefficient data, derived from the balance measurements, illustrate that $C_{L,\max}$ is not significantly increased by low C_μ excitation, regardless of the excitation mode used. This is mainly a result of the inability to control vortex breakdown fully in the vicinity of α_s, as shown in Fig. 14. In contrast, C_D increases substantially in the poststall regime, as a combined result of the simultaneous increase in α and poststall C_N. As expected, C_R shows trends that are similar to C_N, whereas the lateral center of pressure is virtually unaffected. In contrast, C_M is virtually unaltered, and the longitudinal center of pressure movement, away from the apex, was more gradual with excitation.

The efficiency of the excitation in the poststall regime is assessed by considering overall aerodynamic efficiency η and the figure of merit (FM), which represents the ratio of the overall aerodynamic efficiency (taking into account the power consumed by the actuators) to the baseline aerodynamic efficiency.[36] A slight increase in overall aerodynamic efficiency due to the excitation, which manifests as a slightly larger than unity FM, for example, FM = 1.03 for the AM and FM = 1.05 for the BM at incidence of about 40 deg, was measured. This result (FM > 1) is encouraging because it indicates that, even at this flow condition, it is worthwhile introducing power into the actuators, rather than into the power plant, to improve performance. The slightly larger value for FM is associated with the BM excitation results from the relatively large difference in C_E (0.001 for the BM compared to 0.009 for the AM excitation), which is still very small compared to C_D (order 1).

H. Averaged PIV Data

Averaged phase-locked data averaged over a cycle of the modulated low frequency, eight phases acquired PIV data measured at $x/c = 0.25$ and 0.6 for baseline, AM and BM excitation modes are plotted in Fig. 15. Figure 15 presents averaged velocity vectors and essentially streamwise component of averaged vorticity, out-of-the plane perpendicular to the wind-tunnel wall and to the wing upper surface, as shown schematically in Fig. 2. The baseline data acquired at $x/c = 0.25$ (Fig. 15a) suggest the existence of a rather diffused vortical structure, whose size is commensurate with the wing span at this x/c station. AM excitation brings about a tighter average vortex that resides closer to the wing and has a significantly increased circumferential velocity. (The instantaneous vortex may be much tighter but it meanders during the low-frequency modulations.) The BM excitation generates a tighter average vortex, in agreement with the forces and pressures shown in earlier sections.

The baseline data measured at $x/c = 0.6$ do not possess the characteristic features of a typical LE vortex; rather, the flow resembles a detached shear layer with a massive region of almost stagnant flow between the separated shear layer and the wing surface. With excitation, the shear layer deflects toward the wing surface, reestablishing a vortical structure. This is accompanied by a near-wall counterclockwise (positive) vorticity, typical of an attached boundary layer flowing in the negative y/b direction, that is, inboard. The larger

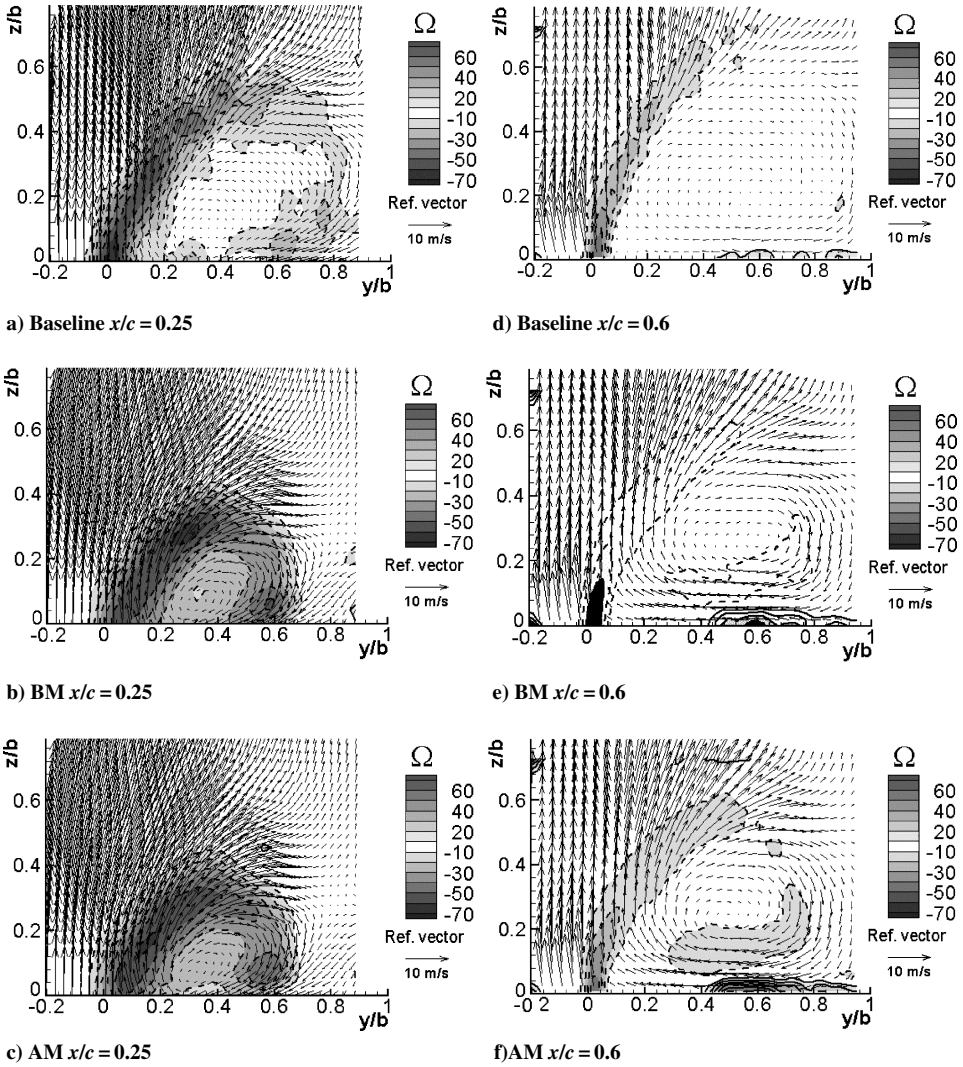

Fig. 15 PIV measured velocity vectors and vorticity contours; $\alpha = 37.8$ deg, $Re = 2.34 \times 10^5$, AM excitation, $F^+ = 2.0$, $C_\mu = 0.4\%$; BM, DCy = 15%, $F^+ = 1.0$, $C_\mu = 0.03\%$.

shear layer deflection and near-wall vorticity associated with the BM excitation is consistent with the larger normal force and lower upper surface pressure observed when using this excitation mode (c.f., Fig. 14).

IV. Conclusions

Zero-mass-flux periodic excitation was applied from internally mounted, segmented, piezoelectric actuators located along the LE of a 60-deg sweptback, semi-span delta wing at poststall angles of attack. The force balance, pressure, and PIV data complement each other and validate the major conclusions, showing significant control authority due to low-frequency modulation of the high-frequency carrier wave.

The effectiveness of the internal actuators could be explained in terms of a nonlinear response of the separated shear layer to the low-frequency modulated excitation signal. This is especially the case where a highly sloped input signal was used, generating a wide frequency response. Namely, BM with very small DCy was found to be more effective than an AM signal that has sine waveform envelope and an order of magnitude larger momentum input.

Several flow indicators suggest that the shear layer separated from the stalled LE resembles a two-dimensional separated flow. The vorticity across the shear layer increases due to enhanced momentum transfer resulting from the introduction of periodic excitation with uniform phase along the entire LE. This in turn generates a flow pattern that resembles the original LE vortex, but whose size is commensurate with the local wing span.

The parametric study leads to the following conclusions. The most effective frequencies were of the order of unity, for example, 1.0 and 2.0 for BM and AM excitation, respectively. Furthermore, high-frequency nonmodulated signals (pure sine waves) resulted in no response or even a slight degradation of aerodynamic performance. The most significant aerodynamic enhancements were achieved at C_μ levels of 0.03 and 0.4% for BM and AM mode, respectively, with corresponding peak slot exit velocities (U_p/U_∞) of 0.7 and 1.3, respectively. The present study does not resolve the open issue of the proper amplitude scaling, that is, excitation momentum or peak velocity. It was found that BM signal that has a low DCy was not only the most effective but also the most energy efficient waveform.

Applying three-dimensional AM excitation, that is, operating all actuators at the same amplitude & frequency but with a controlled phase lag along the LE, degraded performance relative to uniform perturbation without a phase lag. When only one actuator was operated at a time, the improvements in the aerodynamic characteristics were inferior to those achieved while all actuators were operative with the same distributed total C_μ.

Acknowledgment

The experiments were conducted at the Marry and Steve Meadow Aerodynamics Lab., at Tel-Aviv University. Partial support by the Lazarus, Meadow and the Israeli Science Foundation (Equipment Initiation Fund) are gratefully acknowledged.

References

[1]Mitchell, M. A., and Délery, J., "Research into Vortex Breakdown Control," *Progress in Aerospace Sciences*, Vol. 37, No. 4, May 2001, pp. 385–418.

[2]Sheta, E. F., Siegel, J. M., Golos, F. N., and Harrand, V. J., "Twin-Tail Buffet Simulation Using a Multi-disciplinary Computing Environment (MDICE)," *CEAS/AIAA/ICASE/NASA Langley International Forum on Aeroelasticity and Structural Dynamics*, CFD Research Paper Database, June 1999.

[3]Marchman, J. F., III, "Effectiveness of Leading-Edge Vortex Flaps on 60 and 70 Degrees Delta Wings," *Journal of Aircraft*, Vol. 18, No. 4, 1981, pp. 280–286.

[4]Seginer, A., "Experimental Investigation of Vortex Flaps on Thick Delta Wings," *Journal of Aircraft*, Vol. 31, No. 4, 1994, pp. 989, 990.

[5]Kern, S. B., "Evaluation of Turbulence Models for High-Lift Military Aircraft," AIAA Paper 96-0057, Jan. 1996.

[6]Hobbs, C. R., Spaid, F., Ely, W., and Goodman, W., "High Lift Research Program for a Fighter-Type Multi-element Airfoil at High Reynolds Numbers," AIAA Paper 96-0410, Jan. 1996.

[7]Helin, H., and Watry, C. W., "Effects of Trailing-Edge Jet Entrainment on Delta Wing Vortices," *AIAA Journal*, Vol. 32, No. 4, 1994, pp. 802–804.

[8]Shih, C., and Ding, Z., "Trailing Edge Jet Control of Leading-Edge Vortices of a Delta Wing," *AIAA Journal*, Vol. 34, No. 7, 1966, pp. 1447–1457.

[9]Poisson-Quinton, P., "Control du dêcollement d'une sur-face portante par un jet transversal," *Intervention au Congres ICAS*, 1970.

[10]Visser, K. D., Iwanski, K. P., Nelson, R. C., and Ng, T. T., "Control of Leading Edge Vortex Breakdown by Blowing," AIAA Paper 88-0504, 1988.

[11]Guillot, S., Gutmark, E. J., and Garrison, T. J., "Delay of Vortex Breakdown over a Delta Wing via Near Core Blowing," AIAA Paper 98-0315, 1998.

[12]McClean, J. D., Crouch, J. D., Stoner, R. C., Sakurai, S., Seidel, G. E., Feifel, W. M., and Rush, H. M., "Study of the Application of Separation Control by Unsteady Excitation to Civil Transport Aircraft," NASA CR-1999-209338, June 1999.

[13]Oster, D., and Wygnanski, I., "The Forced Mixing Layer Between Parallel Streams," *Journal of Fluid Mechanics*, Vol. 123, 1982, p. 91.

[14]Gad-el-Hak, M., and Blackwelder, R. F., "Control of the Discrete Vortices from a Delta Wing," *AIAA Journal,* Vol. 25, No. 8, 1987, pp. 1042–1049.

[15]Gu, W., Robinson, O., and Rockwell, D., "Control of Vortices on a Delta Wing by Leading-Edge Injection," *AIAA Journal*, Vol. 31, No. 7, 1993, pp. 1177–1186.

[16]Gursul, I., Srinivas, S., and Batta, G., "Active Control of Vortex Breakdown over a Delta Wing," *AIAA Journal*, Vol. 33, No. 9, 1995, pp. 1743–1745.

[17]Deng, Q., and Gursul, I., "Effect of Leading-Edge Flaps on Vortices and Vortex Breakdown," *Journal of Aircraft*, Vol. 33, No. 6, 1996, pp. 1079–1086.

[18]Deng, Q., and Gursul, I., "Vortex Breakdown over a Delta Wing with Oscillating Leading Edge Flaps," *Experiments in Fluids*, Vol. 23, No. 4, 1997, pp. 347–352.

[19]Guy, Y., Morrow, J. A., and McLaughlin, T. E., "Control of Vortex Breakdown on a Delta Wing by Periodic Blowing and Suction," AIAA Paper 99-0132, 1999.

[20]Guy, Y., Morrow, J. A., and McLaughlin, T. E., "Parametric Investigation of the Effects of Active Flow Control on the Normal Force of a Delta Wing," AIAA Paper 2000-0549, 2000.

[21]Traub, L. W., Gilarranz, J. L., and Rediniotis, O. K., "Delta Wing Hingeless Control via Synthetic Jet Actuation," AIAA Paper 2002-0415, 2002.

[22]Huang, A., Folk, C., Silva, C., Chen, Y., Ho, C. M., Jiang, F., Grosjean, C., Tai, Y. C., Lee, G. B., Chen, M., and Newbern, S., "Application of MEMS Devices to Delta Wing Aircraft: From Concept Development to Transonic Flight Test," AIAA Paper 2001-0124, 2001.

[23]Guy, Y., Morrow, J. A., and McLaughlin, T. E., "Velocity Measurements on a Delta Wing with Periodic Blowing and Suction," AIAA Paper 2000-0550, 2000.

[24]Siegel, S. G., Mclaughlin, T. E., and Morrow, J. A., "PIV Measurements on a Delta Wing with Periodic Blowing and Suction," AIAA Paper 2001-2436, 2001.

[25]Siegel, S. G., Mclaughlin, T. E., and Albertson, J. A., "Partial Leading Edge Forcing of a Delta Wing At High Angles of Attack," AIAA Paper 2002-3268, 2002.

[26]Wiltse, J. M., and Glezer, A., "Manipulation of Free Shear Flows Using Piezoelectric Actuators," *Journal of Fluid Mechanics*, Vol. 249, 1993, p. 261.

[27]Amitay, M., Smith, B. L., and Glezer, A., "Aerodynamic Flow Control over an Unconventional Airfoil Using Synthetic Jet Actuators," *AIAA Journal*, Vol. 39, No. 3, 2001, pp. 360–371.

[28]Margalit, S., "Active Flow Control of a Delta Wing at High Incidence Using Segmented Piezoelectric Actuators," M.Sc. Thesis, Dept. of Fluid Mech and Heat Transfer, Tel-Aviv Univ., Tel-Aviv, Jan. 2003.

[29]Papoulis, A., The Fourier Integral and its Applications, McGraw–Hill, New York, 1962, p. 15.

[30]Lachmann, G. V., *Boundary Layer and Flow Control. Its Principles and Application*, Vol. 1–2, Pergamon Press, New York, 1961.

[31]Seifert, A., Bachar, T., Koss, T., Shepshelovich, M., and Wygnanski, I., "Oscillatory Blowing as a Tool to Delay Boundary-Layer Separation," *AIAA Journal*, Vol. 31, No. 11, 1993, pp. 2052–2060.

[32]Seifert, A., Darabi, A., and Wygnanski, I., "Delay of Airfoil Stall by Periodic Excitation," *Journal of Aircraft*, Vol. 33, No. 4, 1996, pp. 691–698.

[33]Greenblatt, D., and Wygnanski, I., "Control of Separation by Periodic Excitation," *Progress in Aerospace Sciences,* Vol. 37, No. 7, 2000, pp. 487–545.

[34]Nishri, B., and Wygnanski, I., "Effects of Periodic Excitation on Turbulent Separation from a Flap," *AIAA Journal*, Vol. 36, No. 4, 1998, pp. 547–556.

[35]Darabi, A., "On the Mechanisms of Forced Flow Reattachment," Ph.D. Dissertation, Dept. of Fluid Mech and Heat Transfer, Tel-Aviv Univ., Tel-Aviv, 2001.

[36]Seifert, A., Eliahu, S., Greenblatt, D., and Wygnanski, I., "Use of Piezoelectric Actuators for Airfoil Separation Control," *AIAA Journal*, Vol. 36, No. 8, 1998, pp. 1535–1537.